# Absolute cross section measurements for the scattering of low- and intermediate-energy electrons from $PF_3$. I. Elastic scattering

N. Hishiyama, M. Hoshino, F. Blanco, G. García, and H. Tanaka

Citation: The Journal of Chemical Physics **147**, 224308 (2017); doi: 10.1063/1.5009482
View online: https://doi.org/10.1063/1.5009482
View Table of Contents: http://aip.scitation.org/toc/jcp/147/22
Published by the American Institute of Physics



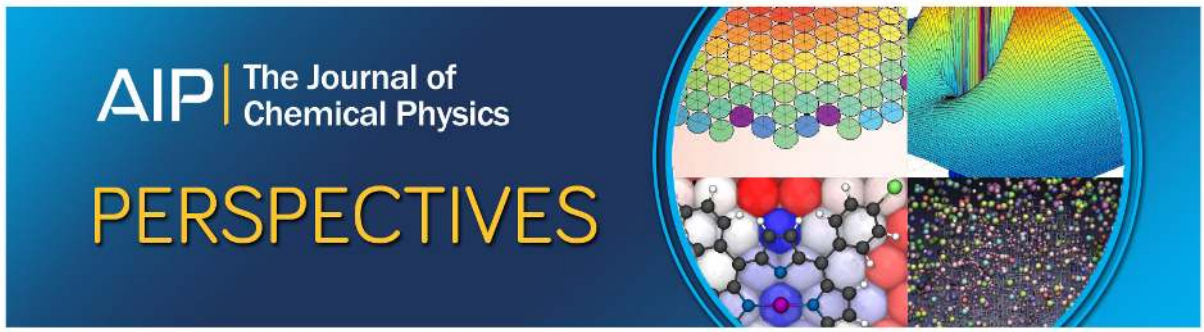

# Absolute cross section measurements for the scattering of low- and intermediate-energy electrons from $PF_3$. I. Elastic scattering

N. Hishiyama,[1] M. Hoshino,[1,a)] F. Blanco,[2] G. García,[3] and H. Tanaka[1]
[1]*Department of Physics, Sophia University, Chiyoda-ku, Tokyo 102-8554, Japan*
[2]*Departamento de Fisica, Atomica, Molecular y Nuclear, Facultad de Ciencias Fisicas, Universidad Complutense de Madrid, E-28040 Madrid, Spain*
[3]*Instituto de Fisica Fundamental, Consejo Superior de Investigaciones Científicas, 28006 Madrid, Spain*

(Received 17 October 2017; accepted 27 November 2017; published online 13 December 2017)

We report absolute elastic differential cross sections (DCSs) for electron collisions with phosphorus trifluoride, $PF_3$, molecules ($e^- + PF_3$) in the impact energy range of 2.0–200 eV and over a scattering angle range of 10°–150°. Measured angular distributions of scattered electron intensities were normalized by reference to the elastic DCSs of He. Corresponding integral and momentum-transfer cross sections were derived by extrapolating the angular range from 0° to 180° with the help of a modified phase-shift analysis. In addition, due to the large dipole moment of the considered molecule, the dipole-Born correction for the forward scattering angles has also been applied. As a part of this study, independent atom model calculations in combination with screening corrected additivity rule were also performed for elastic and inelastic (electronic excitation plus ionization) scattering using a complex optical potential method. Rotational excitation cross sections have been estimated with a dipole-Born approximation procedure. Vibrational excitations are not considered in this calculation. Theoretical data, at the differential and integral levels, were found to reasonably agree with the present experimental results. Furthermore, we explore the systematics of the elastic DCSs for the four-atomic trifluoride molecules of $XF_3$ (X = B, N, and P) and central P-atom in $PF_3$, showing that, owing to the comparatively small effect of the F-atoms, the present angular distributions of elastic DCSs are essentially dominated by the characteristic of the central P-atom at lower impact energies. Finally, these quantitative results for $e^- - PF_3$ collisions were compiled together with the previous data available in the literature in order to obtain a cross section dataset for modeling purposes. To comprehensively describe such a considerable amount of data, we proceed by first discussing, in this paper, the vibrationally elastic scattering processes whereas vibrational and electronic excitation shall be the subject of our following paper devoted to inelastic collisions. *Published by AIP Publishing.*
https://doi.org/10.1063/1.5009482

## I. INTRODUCTION

Cross section data for electron-molecule scattering play an important role to understand the electron transport properties and electron energy distribution in electron swarm applications through various gases. Fluorine compound molecules have been widely used in plasma-assisted fabrication of large-scaled-integrated circuits, semiconductor manufacturing, surface hardening, and other technological applications.[1] For example, although either pure phosphorous or its halides or hydrides, i.e., phosphane ($PH_3$) molecules, have been used in micro-electronic doping of phosphorous, these samples are highly toxic and flammable. Thus, phosphorus trifluoride, $PF_3$, molecules, have been suggested to be a replacement sample for gas phase synthesis in micro-electronic doping.[2] However, experimental or theoretical studies of internal reactions in plasmas containing $PF_3$ have not kept pace with their application usages.

A literature survey shows that previous experimental and theoretical studies on low- and intermediate-energy electron scattering from $PF_3$ molecules are quite restricted to specific topics. Previous studies include electron impact formation of positive and negative ions from $PF_3$ in the gas phase[3–5] and total cross section (TCS) as measured by Szmytkowski *et al.*[6] in the electron energy range 0.5–370 eV. Au *et al.*[7] reported absolute photoabsorption oscillator strengths for valence and inner shell excitations of $PF_3$ by using dipole (e, e) spectroscopy in the excitation energy range from 5 to 300 eV. On the theoretical side, Shi *et al.*[8] calculated electron scattering TCS for eight target molecules including $PF_3$ at the Hartree-Fock level by means of a modified additivity rule (AR) approach. Moreover, Vinodkumar *et al.*[2] reported TCS values for $PF_3$ calculated by an *ab initio* treatment using Quantemol-N which utilizes the UK molecular R-matrix code (hereafter, the R-matrix code) for impact energies ranging from 0.1 to 15 eV and using the spherical complex optical potential (SCOP) formalism from the ionization threshold up to 5000 eV. These results included rotationally resolved and rotational-summed elastic differential and integral cross

a)Author to whom correspondence should be addressed: masami-h@sophia.ac.jp. Tel.: (+81) 3 3238 4227. Fax: (+81) 3 3238 3341.

sections (DCSs and ICSs) for $PF_3$ at impact energies in the 0.32–19 eV range, integral electronic excitation cross sections for the first three excited states (3A″, 3A′, and 1A″), and total ionization cross sections from the ionization threshold to 5000 eV by using both complex scattering potential ionization contribution (CSP-IC) analysis and the binary encounter Bethe method (see Ref. 2 for details). Furthermore, in this calculation, three prominent structures were predicted in the TCS; the Ramsauer-Townsent (R-T) minimum at 0.33 eV, a shape resonance (2A″) at 0.77 eV, and a Feshbach resonance (2A′) at 13.57 eV, respectively.[2] More recently, Kumar[9] reported theoretically partial single- and double-differential cross sections through the study of direct and dissociative electron impact ionization of $PF_3$ for electron incident energies of 100 and 200 eV using the modified Jain-Khare semi-empirical approach. However, no DCS measurement for vibrationally elastic and inelastic (vibrational and electronic excitations) cross sections in $PF_3$ has been reported for electron energies below 100 eV, which are crucial for plasma modeling studies. Hence, the first motivation for the present investigation is to fulfill, at least in part, this current literature gap.

Here we, therefore, present experimental absolute elastic DCS data for $PF_3$ (classified into the $C_{3v}$ group symmetry) in the energy range from 2.0 to 200 eV. Corresponding ICS and momentum-transfer cross sections (MTCSs) are also provided by extrapolating the DCSs with the help of a modified phase-shift analysis (MPSA) including the dipole-Born correction to the forward scattering amplitude due to the large permanent dipole moment of this molecule. We also report cross section results from an independent atom model calculation in combination with the screening corrected additivity rule (IAM-SCAR), based on a complex optical potential method and complemented with the dipole-Born approximation to account for molecular rotations. The overall procedure provides differential and integral elastic and rotational excitation cross sections as well as integral inelastic (electronic excitation and ionization) cross sections. Vibrational excitations are not considered in this calculation. Another justification of this study is that the $PF_3$ molecule is an intrinsically interesting molecule from the fundamental point of view. Hence, we explore the systematics of the elastic DCSs for the four-atom trifluoride, $XF_3$ (X = B, N, and P) molecules in a similar way as that discussed in our previous series of studies.[1,10–13] The present comparison shows that these elastic DCSs are independent of the nature of the central X atoms at the vertex of $XF_3$ (X = B, N, and P) above 30 eV, while their own chemical and physical properties begin to emerge clearly in the DCSs below 10 eV. Finally, TCS values have also been estimated by adding the total inelastic cross sections calculated by the IAM-SCAR and the measured vibrational inelastic cross sections (see Ref. 14) to the present elastic ICS. These estimated values are presented here as the "experimental total cross sections." All these results, together with the previous data available in the literature, are compiled to obtain an $e^- - PF_3$ collisional cross section dataset for plasma modeling applications.

In Sec. II, we provide details of the experimental apparatus and procedures used for the present measurements. In Sec. III, we present a brief description of our differential and integral cross section calculation methods and the extrapolation procedures applied to the elastic DCSs in order to obtain the ICS and MTCS. In Sec. IV, the experimental data for elastic scattering are presented and discussed in comparison with other previous available studies. Finally, some conclusions that can be drawn from the present study are given in Sec. V.

## II. EXPERIMENTAL DETAILS

The present experiments were performed using two different crossed-beam spectrometer configurations. The original spectrometer has been described in detail elsewhere,[15] while a description of the newer one was given by Kato *et al.*[16] Both spectrometers consist of a combination of hemispherical monochromators and analyzers. In both cases, differentially pumped electron lens systems to transport and focus the electron beam are controlled by computer-driven voltages. Well-characterized and well-understood electron optics are crucial in this investigation, particularly in relation to the measurements of electron energy loss spectra (see Fig. 1). Great care was therefore exercised, with our standard measurement techniques being given in detail by Tanaka *et al.*[17] In this study, the electron beam emerging from the electrostatic hemispherical monochromator collides with an effusive molecular beam of $PF_3$ at right angles. Electrons scattered in a certain scattering angle are energy-analyzed by a second electrostatic hemispherical analyzer.

For the elastic scattering measurements, the original spectrometer operated at fixed incident electron energies between

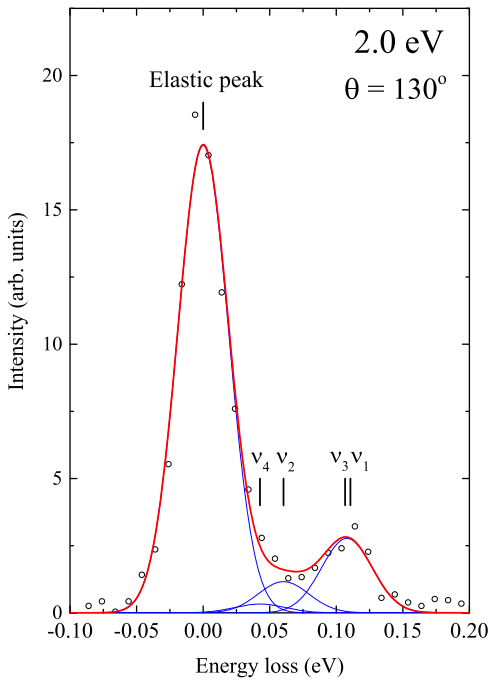


FIG. 1. Typical energy loss spectrum of scattered electrons from $PF_3$ at an impact energy of 2.0 eV and at a scattering angle of 130° with an energy-resolution of ~40 meV. The elastic peak and low-lying fundamental vibrational-modes, $\nu_1$ (110.6 meV), $\nu_2$ (60.4 meV), $\nu_3$ (106.6 meV), and $\nu_4$ (42.7 meV),[18] are shown as bar plots.

2.0 and 40 eV and over the scattered electron angular range 10°–130°. The overall energy resolution achieved with this setup was typically within 40–45 meV (FWHM) for electron incident electron currents of the order of 3–6 nA, which may be sufficient to resolve contributions from the lower vibrational modes, $\nu_1 + \nu_3$ (110 meV and 106 meV) of $PF_3$ to the measured elastic signal, but not enough to distinguish those from either the $\nu_2$ (60 meV) or $\nu_4$ (42 meV) vibrational channels[18] as well as from the rotational excitations (see Table I and Fig. 1). However, even with the present energy resolution, it is clear from Fig. 1 that the contributions of these vibrational excitations to the elastic scattering are relatively small. The latter spectrometer was operated at 60, 100, and 200 eV impact energies with incident electron current of 5–7 nA and covering the scattered electron angular range from 10° to 150°. In this case, though the energy resolution was relaxed to ~100 meV (FWHM), at these relatively high energy regions, the vibrational excitation cross sections are expected to be so small that any contributions of those channels to the elastic signal can be safely ignored.

Energy scales of both spectrometers were calibrated by measuring the $He^-$ $1s2s^2\ ^2S$ Feshbach resonance at 19.37 eV.[19] The first peak of vibrational excitation, $v = 0 \rightarrow 1$, of the $^2\Pi_g$ shape resonance of $N_2$ at 1.97 eV[20] was also used for the energy calibration of the former setup at the lower impact energies, below 10 eV. For both systems, the angular scales, with resolutions within ±1.5°, were calibrated from the symmetry of the angular distribution of the line profile corresponding to the He $1s^2\ ^1S \rightarrow 1s2p\ 2^1P$ inelastic excitation as measured by changing the scattering angle form $+\theta$ to $-\theta$ with respect to the nominal-scattering angle $\theta = 0°$. The molecular beam was produced effusively from a tube nozzle of 5-mm length and 0.3-mm diameter, which was kept at a relatively high temperature (~70 °C) throughout the measurements to avoid surface contamination on the nozzle from $PF_3$ molecules. The $PF_3$ sample was supplied from Takachiho Chemical Industrial Co., LTD. with a stated purity better than 99.9%.

In this study, the elastically scattered electron signals have been converted into absolute cross sections by normalizing to the standard elastic DCS of He,[21] using the well-established relative flow technique.[22–25] This normalization requires using the constant Knudsen number of $PF_3$ and He to generate equal two gas densities of both targets in the collision volume. Head pressures behind the nozzle of about 0.6 Torr for $PF_3$ and 1.8 Torr for He, respectively, were obtained from the molecular diameters derived from the hard sphere model (diameters of ~3.8 Å and 2.18 Å, respectively).

Finally, the experimental uncertainties of the present measurements are estimated to be within 10%–15% for the elastic scattering DCS results and within 26%–28% for the integral cross sections (ICSs) and momentum-transfer cross sections (MTCSs). These uncertainty limits associated with the present experimental data are estimated as follows: the normalization procedure using He reference data is accurate to about 15%, the scattered electron counting procedure introduces a statistical uncertainty of about 3% for the elastic scattering and up to 10% for the inelastic scattering, and the DCS extrapolation process is estimated to contribute with an additional ~15%. These extrapolation procedures will be discussed in Sec. III B.

TABLE I. Physical and chemical properties of $XF_3$ (X = P, N, and B).[18,33–35]

| | $PF_3$ | $BF_3$ | $NF_3$ |
|---|---|---|---|
| Symmetry | $C_{3v}$ | $D_{3h}$ | $C_{3v}$ |
| X-F bond length (Å) | 1.57 | 1.31 | 1.37 |
| F-X-F angle (deg) | 97.8 | 120 | 102 |
| Polarizability (Å$^3$) | 4.43 | 3.31 | 2.81 |
| Dipole moment (D) | 1.03 | 0 | 0.24 |
| Ionization potential (eV) | 11.38 | 15.70 | 12.94 |
| Fundamental modes (meV) | | | |
| $\nu_1$ (symmetry stretching) | 110.6 | 110.1 | 128.0 |
| $\nu_2$ (symmetry deformation) | 60.4 | 85.7[a] | 80.2 |
| $\nu_3$ (degenerate stretching) | 106.6 | 179.7 | 112.5 |
| $\nu_4$ (degenerate deformation) | 42.7 | 59.5 | 61.0 |

[a]out-of-plane-deformation for $BF_3$.

## III. THEORETICAL APPROACH, FITTING, AND INTEGRATION PROCEDURE

### A. IAM-SCAR calculation

Details of the application of the independent atom model under the screening corrected additivity rule (IAM-SCAR) method[26,27] to electron interactions have been provided in a number of recent papers from our group.[1,10–13] Briefly, each atomic target (F and P) is represented by an interacting complex potential (so-called optical potential). The real part accounts for the elastic scattering of the incident electrons, and the imaginary part represents the inelastic processes, which are considered as "absorption" from the incident electron beam. For the elastic part, the potential is represented by the sum of three terms: (a) a static term derived from a Hartree-Fock calculation of the atomic charge density distribution, (b) an exchange term to account for the indistinguishability of the incident and target electrons, and (c) a polarization term for the long-range interactions which depends on the target polarizability. The inelastic scattering, on the other hand, is treated as electron-electron collisions within a target electron cloud restricted by the appropriate boundary conditions. Further improvements to the original formulation in the description of the electron's indistinguishability and the inclusion of screening effects led to a model which provides a good approximation for electron-atom scattering over a broad energy range. To calculate the cross sections for collision with $PF_3$, the additivity rule (AR) is then applied to the optical model results for each constituent atom. In this approach, the molecular scattering amplitude results from the coherent sum of all the relevant atomic amplitudes, which gives the DCSs for the molecule of interest. ICS can be determined by numerically integrating those DCS from 0° to 180°. The geometry of the molecule (atomic positions and bond lengths) is taken into account by using some screening coefficients and this enables the range of validity of the technique to be extended down to electron impact energies ~30 eV (or lower). This

procedure provides differential and integral elastic cross section as well as integral inelastic (electronic excitations plus ionization) cross sections. Nuclear movements are not considered in this approach. However, additional differential and integral rotational cross sections are calculated by considering dipole interactions within the framework of the Born approximation.

### B. Fitting and integrating procedure

Figure 1 shows a typical electron energy loss (EEL) spectrum of $PF_3$ at an impact energy of 2.0 eV and scattering angle of 130° including both elastic scattering and vibrational excitations of fundamental modes as recorded with the apparatus described above and operating with an energy resolution of ~40 meV. As shown in Fig. 1, our spectral deconvolution procedures enable us to separate out the elastic peak from those for vibrational excitations. With the present energy resolution of 40–45 meV, the tail of the elastic peak overlaps the lowest vibrational excitation peak just on the energy-loss side. For the present deconvolution process, this tail has been subtracted with the help of the similar tail corresponding to the observed elastic peak of He, while Gaussian profiles for both the elastic scattering and the four fundamental vibrational modes of the observed EEL spectra have been considered (see Fig. 1). This standard spectral deconvolution procedure[17] allowed, for each impact energy, extracting the individual cross section contribution of the fundamental vibrational modes. More details on the vibrational excitation cross section measurements will be described in Ref. 14.

In order to obtain the experimental ICS and MTCS, the present measured elastic DCSs were extrapolated for scattering angles $\theta < 10°$ and $130° < \theta$ by using either the theoretical angular distributions of the present IAM-SCAR calculations (above 30 eV) or a modified phase shift analysis (MPSA), including polarization and Born correction[28] for the higher order phase shifts (below 20 eV). For this approach, Thompson's formulation of the Born approximation[29] has been used by assuming the polarizability of $PF_3$[30] as $\alpha = 4.43$ Å$^3$. In addition, the dipole-Born cross sections formulated by Itikawa[31] has been added to the forward scattering amplitudes in the energy range 2.0–20 eV. Following these fitting procedures, DCS values for the full angular range, i.e., from 0° to 180°, were obtained as plotted in Fig. 2. Note that we assumed a minimum energy loss of 0.07 meV, corresponding to the rotational excitation energy from J = 0 to 1,[2] to prevent the dipole-Born singularity at 0° scattering angle. Once the elastic DCSs were extrapolated with either of the

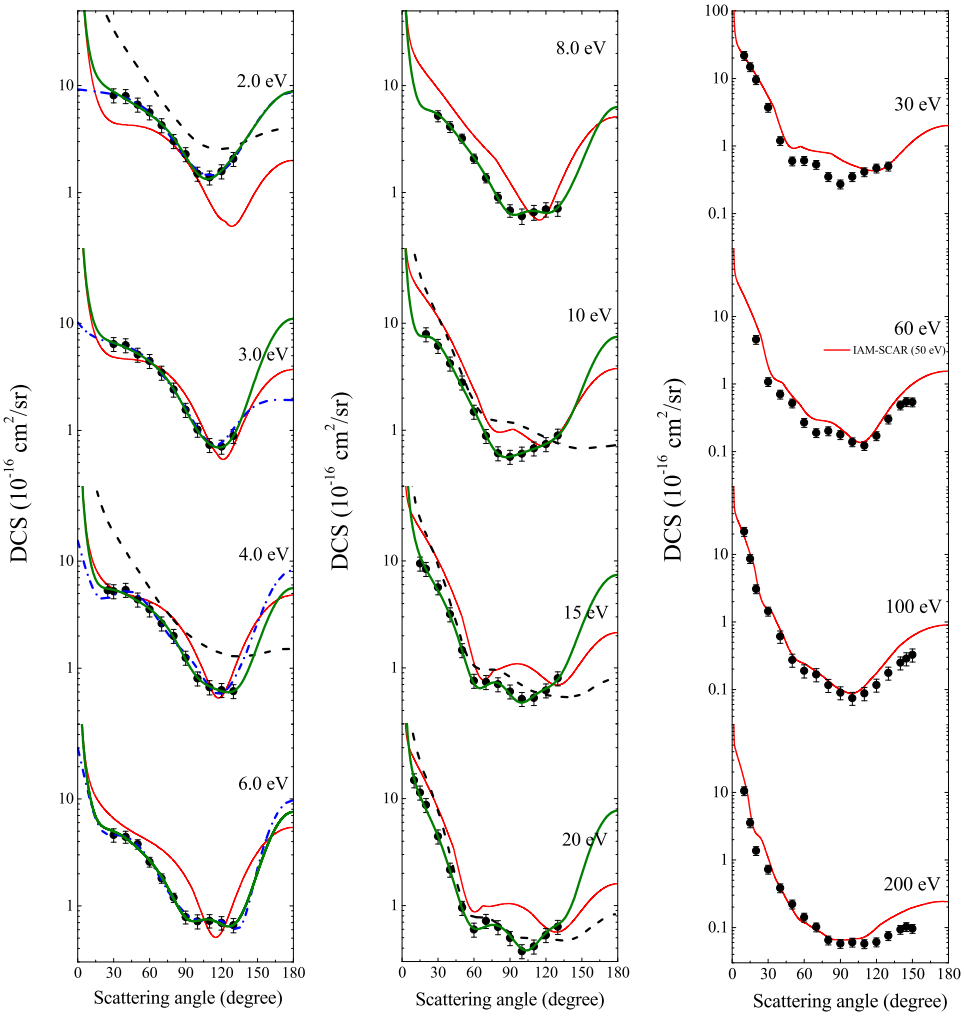


FIG. 2. Elastic differential cross sections for $PF_3$ in the impact energy region 2.0–200 eV, together with the present IAM-SCAR calculation, MPSA fitting results[28] combined with the dipole-Born cross sections,[31] and previous theoretical calculations. (•) present measurements, blue dashed-dotted and green solid lines present MPSA fitting without and with the dipole-Born DCS, respectively. Red thin solid lines: IAM-SCAR calculations. Black dashed lines: previous elastic DCSs calculated using the *ab initio* R-matrix code.[2]

TABLE II. Elastic differential ($10^{-16}$ cm$^2$/sr), integral cross sections, ICS ($10^{-16}$ cm$^2$) and momentum-transfer cross sections, MTCS ($10^{-16}$ cm$^2$) for $PF_3$. Uncertainties on the DCS are typically 10%–15%, on ICS and MTCS ~26%–28%.

| | Impact energy (eV) | | | | | | | | | | | | |
|---|---|---|---|---|---|---|---|---|---|---|---|---|---|
| Angle (deg) | 2.0 | 3.0 | 4.0 | 6.0 | 8.0 | 10 | 15 | 20 | 30 | 40 | 60 | 100 | 200 |
| 10 | ... | ... | ... | ... | ... | ... | ... | 14.84 | 21.78 | 26.23 | 17.32 | 21.76 | 10.50 |
| 15 | ... | ... | ... | ... | ... | ... | 9.468 | 11.40 | 14.84 | 16.21 | 9.947 | 8.642 | 3.536 |
| 20 | ... | ... | ... | ... | 5.209 | 7.901 | 8.427 | 8.712 | 9.530 | 9.682 | 4.542 | 3.075 | 1.366 |
| 25 | ... | ... | 5.332 | ... | ... | ... | ... | ... | ... | ... | ... | ... | ... |
| 30 | 8.122 | 6.416 | 5.236 | 4.604 | 4.123 | 6.160 | 5.663 | 4.432 | 3.718 | 2.525 | 1.075 | 1.440 | 0.724 |
| 40 | 7.995 | 6.254 | 5.394 | 4.426 | 3.206 | 4.205 | 3.172 | 2.166 | 1.195 | 0.907 | 0.702 | 0.609 | 0.384 |
| 50 | 6.651 | 5.104 | 4.388 | 3.776 | 2.082 | 2.797 | 1.467 | 0.952 | 0.598 | 0.761 | 0.519 | 0.273 | 0.221 |
| 60 | 5.627 | 4.456 | 3.546 | 2.580 | 1.368 | 1.489 | 0.758 | 0.597 | 0.606 | 0.625 | 0.268 | 0.190 | 0.142 |
| 70 | 4.268 | 3.469 | 2.619 | 1.810 | 0.902 | 0.885 | 0.739 | 0.719 | 0.531 | 0.393 | 0.189 | 0.167 | 0.102 |
| 80 | 3.036 | 2.407 | 2.001 | 1.197 | 0.678 | 0.609 | 0.703 | 0.629 | 0.349 | 0.237 | 0.201 | 0.116 | 0.065 |
| 90 | 2.291 | 1.558 | 1.251 | 0.786 | 0.602 | 0.564 | 0.602 | 0.497 | 0.272 | 0.278 | 0.177 | 0.090 | 0.058 |
| 100 | 1.504 | 1.016 | 0.802 | 0.719 | 0.656 | 0.604 | 0.513 | 0.374 | 0.350 | 0.348 | 0.138 | 0.075 | 0.060 |
| 110 | 1.388 | 0.732 | 0.664 | 0.725 | 0.697 | 0.677 | 0.523 | 0.415 | 0.413 | 0.370 | 0.122 | 0.088 | 0.057 |
| 120 | 1.583 | 0.706 | 0.624 | 0.696 | 0.709 | 0.742 | 0.616 | 0.530 | 0.468 | 0.394 | 0.171 | 0.117 | 0.061 |
| 130 | 2.072 | 0.889 | 0.610 | 0.662 | 0.733 | 0.891 | 0.799 | 0.633 | 0.502 | 0.482 | 0.302 | 0.176 | 0.075 |
| 140 | ... | ... | ... | ... | ... | ... | ... | ... | ... | ... | 0.485 | 0.249 | 0.093 |
| 145 | ... | ... | ... | ... | ... | ... | ... | ... | ... | ... | 0.545 | 0.287 | 0.102 |
| 150 | ... | ... | ... | ... | ... | ... | ... | ... | ... | ... | 0.540 | 0.327 | 0.096 |
| *ICS* | 60.10 | 44.86 | 33.40 | 29.19 | 26.34 | 26.54 | 27.96 | 22.00 | 17.59 | 18.00 | 12.40 | 9.50 | 4.92 |
| *MTCS* | 40.60 | 30.40 | 19.98 | 19.55 | 17.37 | 18.57 | 16.98 | 14.75 | 8.68 | 8.26 | 4.49 | 2.62 | 1.23 |

above fitting procedures, numerical integration of the DCSs from 0° to 180°[32] yielded the present ICS and MTCS results. These values are shown at the foot of Table II and plotted in Fig. 5.

## IV. RESULTS AND DISCUSSION

In this section, from Subsections IV A–IV C, the present experimental results are compared and discussed with previous data available in the literature. Some physical properties and the vibrational excitation energies of the fundamental modes of $XF_3$ (X = B, N, and P) are summarized in Table I [17,33–35] for comparison.

### A. Elastic DCSs for $e^-$ + $PF_3$ from 2.0 to 200 eV

Figure 2 shows the absolute elastic DCS for $PF_3$ obtained using the relative flow technique at electron impact energies from 2.0 to 200 eV for scattering angles ranging from 10° to 150°. The corresponding results of the present IAM-SCAR calculations from 2.0 to 200 eV incident energies are also plotted in Fig. 2, together with the MPSA fitting results to the present measured DCSs between 2.0 and 20 eV in the full angular range, i.e., from 0° to 180°, without and with dipole-Born correction to the forward scattering cross sections. Recently published calculated elastic DCSs by Vinodkumar *et al.*[2] using the R-matrix method are also plotted in Fig. 2 from 2.0 to 19 eV incident electron energies.

As can be seen in Fig. 2, for the lower impact energies between 2.0 and 4.0 eV, the angular distributions seem to be dominated by the p-wave scattering with a (shoulder) plateau around 50° and a single minimum near 110°. No important contributions from higher order partial waves to the present results can be expected in this energy region. As the electron energy increases up to 10 eV, the flat zone becomes gradually narrower getting closer to the smaller angles and the minimum covers a broader angular region between 90° and 130°. At impact energies from 15 eV to 30 eV, the contribution of d-waves should be noticeable around the minimum of the DCSs. The angular distribution, therefore, shows a local maximum about 80° between two minima at 60° and 90°, respectively. For higher incident energies, above 60 eV, due to the interference contributions from higher order partial waves, undulations tend to disappear giving a continuum which deceases very rapidly with increasing angles. In general, DCSs tend to peak in the forward direction when the incident energy increases but, in particular, this effect is magnified for polar molecules having also relatively large polarizabilities, as in the case of $PF_3$ ($\mu = 1.03$ D, $\alpha = 4.43$ Å$^3$).[30] This feature is clearly shown in Fig. 2 by our MPSA fitting results. Considering Thompson's correction to include the higher order phase shifts and the value of the polarizability (results without dipole-Born correction to the forward scattering cross sections), this forward peaking becomes visible above 4.0 eV. Furthermore, when the permanent dipole of the molecules is considered (results with dipole-Born correction), the small scattering angle enhancement mainly affects the lower energies.

Perhaps the most remarkable feature of Fig. 2 is the good qualitative agreement between our IAM-SCAR calculation and the measured DCSs even at low impact energies such as 2.0 eV. As expected from our previous papers, there is a general quantitative agreement for incident energies $E_0 \geq 50$ eV between our theoretical and experimental values. However, in the case of $PF_3$ our calculated DCS reproduces reasonably well

the observed angular distribution of scattered electrons even down to 2.0 eV. Other important consequence of this comparison is that although the dipole interaction affects mainly the smaller scattering angles, not experimentally accessible, dipole interactions need to be considered both in the IAM-SCAR calculation and the MPSA fitting procedure[31] in order to obtain a proper agreement with the experimental values. Note that this modifies substantially the derived integral cross section as well as the momentum transfer cross section values which tend to be much higher when dipole interactions are included. It is also noteworthy that the backward peaking below 6.0 eV, which was found in other polar molecular targets,[36,37] is not evident from the present measurements. This larger angle region also contributes to the determination of the ICS and the MTCS and therefore calculated and extrapolated values can be again crucial. Further experimental verification is needed for the forward and the backward scattering angles.

On the other hand, the elastic DCS values calculated by Vinodkumar *et al.*[2] with an R-matrix procedure are clearly different than the experimental ones at the lower impact energies, below 10 eV. They show much better agreement for higher energies from 15 to 20 eV. The R-matrix method usually provides a reasonable approximation to the scattering problem giving the appropriate shape of the elastic DCSs, especially for low impact energies. In the case of $PF_3$, the disagreement between the present experimental results and those calculated in Ref. 2 may arise from the target molecule representation assumed by Vinodkumar *et al.*[2] In fact, their calculated dipole moment of 3.44 D[2] is quite large in comparison with the experimental value of 1.03 D reported in Ref. 35. This can lead to an overestimation of the rotational excitation ($J = 0 \rightarrow 1$) cross section. Note that the dipole moment is very sensitive to the basis set chosen on the surface of the R-matrix sphere which may also affect to the pure elastic scattering ($J = 0 \rightarrow 0$) cross section.

In addition, two resonances have been predicted by the R-matrix calculation[2] at 0.776 eV of width 0.902 eV and 13.57 eV of width 1.157 eV, respectively. The former resonance indicates the dominance of p-wave in the partial wave interference pattern below 1 eV. On the other hand, as shown in Sec. IV B, the p-wave behavior observed in the DCS for low impact energies resembles the scattering amplitude distribution from the single center potential of the constituent atoms and, in particular, that corresponding to the central phosphor-atom of $PF_3$ (see Fig. 4). This characteristic angular distribution is also confirmed by the present IAM-SCAR calculation which does not intrinsically predict resonances. This indicates that information on resonances extracted from the elastic DCSs of $PF_3$ can be obscured by the intrusion of the direct scattering, i.e., dominant p-wave scattering, from the central P atom; thus, a complementary study of the vibrationally inelastic scattering would be necessary (see Ref. 14).

### B. Comparison of the angular distributions of the $XF_3$ (X = B, N, and P) DCSs

In our previous study,[1] a comparison between the measured DCSs and those calculated with the IAM-SCAR for molecules containing three fluorine atoms, $XF_3$ (X = B, C, N, and CH), was performed showing that atomic fluorine was mainly responsible for the similarities and differences in magnitude and shape of the corresponding elastic DCSs (see Ref. 1 for details). Here, Figs. 3(a)–3(d) show comparisons of the observed angular distributions for the three considered trifluoride molecules ($PF_3$, $NF_3$, and $BF_3$) at impact energies of 3.0, 8.0, 30, and 100 eV over the scattering angles from 0° to 180°. Our corresponding IAM-SCAR calculations are also plotted in Figs. 3(a)–3(d). Furthermore, in Figs. 4(a) and 4(b), we compare our experimental DCSs for three different trifluoride molecules, $XF_3$ (X = P, N, and B), with our model potential calculation results for each central atom (P, N, B) together with those for the F atom, multiplied by 3 (F × 3), at impact energies of 3.0 and 8.0 eV.

$PF_3$ and $NF_3$ are polar molecules, assigned to the equilateral triangular pyramid geometry ($C_{3v}$) with the central atom at the vertex and three F atoms at the corners of the bases, whereas $BF_3$ is a non-polar molecule assigned to the trigonal planar geometry ($D_{3h}$) with symmetric charge distribution on the central X atom. Note that in the former two cases, there is one pair of lone pair electrons on the central X atoms. Based on the valence shell electron pair repulsion (VSEPR) theory,[38] the electron clouds and the lone pair electron around the central X atom will repel each other. As a result, they will be pushed apart giving the $PF_3$ and $NF_3$ molecules a trigonal pyramidal molecular geometry or shape.

At first sight, Figs. 3(a) and 3(b) show a different behavior of the DCS of $PF_3$, $NF_3$, and $BF_3$ at 3.0 and 8.0 eV, while Figs. 3(c) and 3(d) show how they tend to be similar for the higher impact energies of 30 and 100 eV. This comparison reveals that molecular properties are important at 3.0 eV, due to the nature of the chemical binding, leading usually to a considerable anisotropic distortion of the electron charge distribution. Note that dipole moments of $PF_3$ and $NF_3$ are only effective for small scattering angles below 10°. Furthermore, elastic DCSs of $NF_3$ exhibit a broad maximum around 40° and a single minimum near 100° which is reproduced by the present IAM-SCAR calculation rather well even at 3.0 eV in the scattering angle ranges from 20° to 130°. On the other hand, $BF_3$ presents a rather flat angular distribution, which is not reproduced by the present IAM-SCAR calculation. Here, it must be remembered that the R-T effect expected at ~1.5 eV[1,39] for $BF_3$ still remains for energies about 3.0 eV, where s-wave dominates, thus giving an isotropic angular distribution of elastic DCS. As mentioned before, from our previous experiences,[1] agreement between our experimental and theoretical data can be expected for energies above 20 eV. The excellent agreement found for $PF_3$ and $NF_3$ at 3.0 eV is probably due to the particular charge distribution of these molecules and cannot be generalized to other molecules. As the IAM-SCAR approach is initially based on the scattering from each atomic center, the DCSs for the constituent atoms, P, N, B, and F (×3), are also plotted in Figs. 4(a) and 4(b) to be compared with the corresponding molecules. As mentioned above, the angular distribution of the DCS of $PF_3$ seems to be strongly influenced by the central P atom and is dominated by p-wave scattering, whilst the F (×3) atoms present an almost flat contribution. A closer inspection indicates that there are some differences with respect to the magnitude of the depth of the

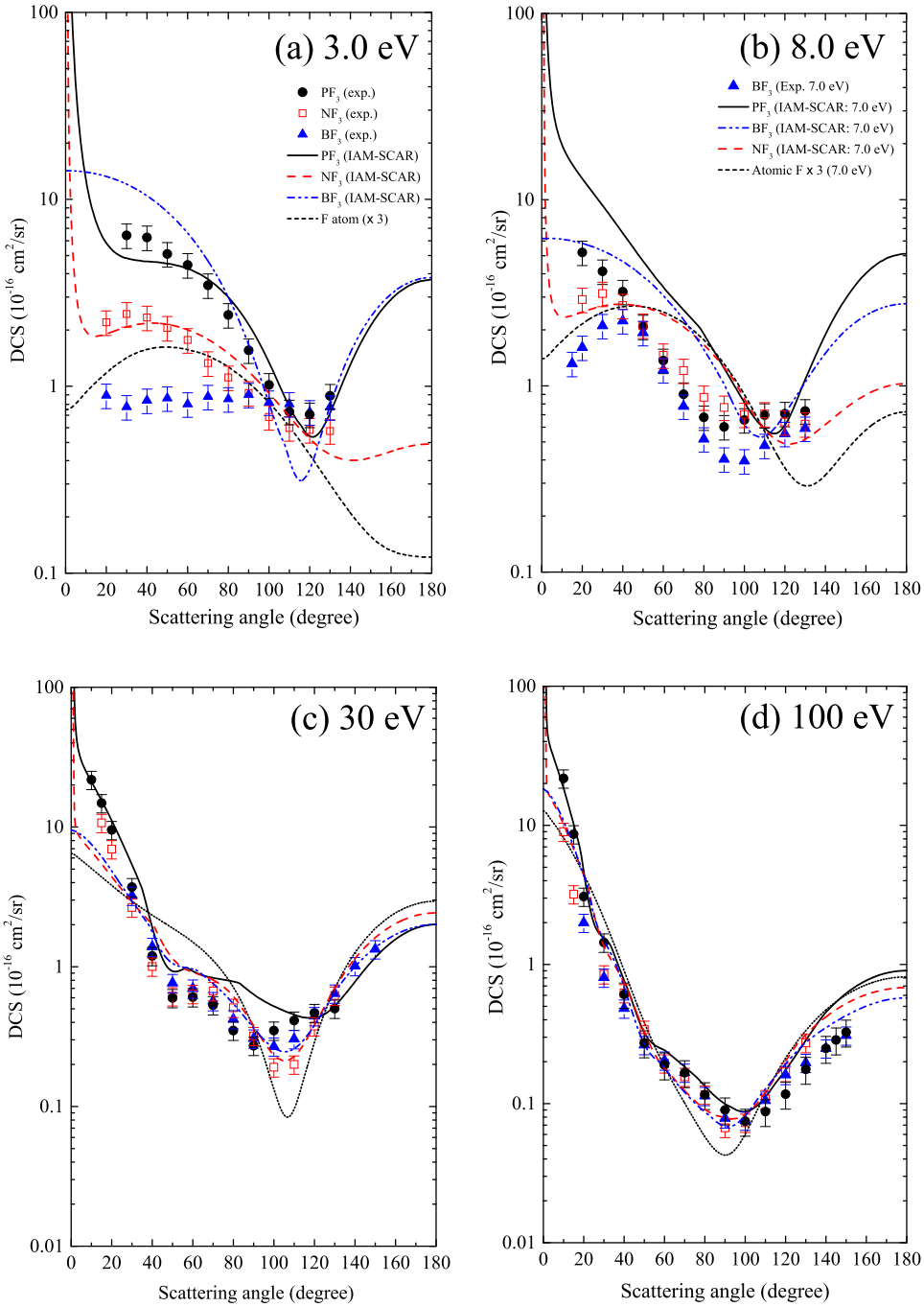


FIG. 3. Comparison of the present DCSs for $PF_3$ with those for $XF_3$ (X = B, C, and N) molecules[1] as well as calculated results for atomic-fluorine multiplied by factor of 3 in order to demonstrate the effect of three fluorine atoms in the $PF_3$ molecule at (a) 3.0 eV, (b) 8.0 eV, (c) 30 eV, and (d) 100 eV (see legends for details).

critical minimum around 100° and the deceasing trend in the forward scattering, suggesting that "molecular effects" play a more important role in these angular regions. A similar situation is found for $NF_3$ at least qualitatively, where the trend in the forward scattering shifts now by about 15° and again deviates for the larger scattering angles. For $BF_3$, however, the DCS angular distribution is clearly different than the calculated distributions for B and F (×3) atoms. This smoother feature may arise from the high degree of symmetry of the trigonal planar structure ($D_{3h}$) assigned to this molecule. A similar situation appears for $CH_4$ with $T_d$ symmetry.[28] This molecule is randomly oriented in the gas-phase, resulting that a scattering field is nearly spherical. Though a weak p-wave shape resonance ($B_2$ symmetry) has been predicted theoretically around 3.8 eV,[39] which was also observed in our measurements, any features characterized by this shape resonance were not appreciable experimentally in the angular distributions of elastic DCS below 3.5 eV.[1] Therefore, it suggests that the R-T effect was more dominant than the shape resonance in this energy range.

As the electron energy increases, the DCS becomes more peaked in the forward direction, which is a manifestation of the fact that more partial waves contribute to the scattering process. At 8.0 eV, in the case of $BF_3$, a broad undulation extends over the angular distribution with a maximum at 40° and a minimum around 90°. As a result, the DCSs for the three considered molecules overlap around 60°, showing that the shoulders are shifted over the smaller angles and the minima located over

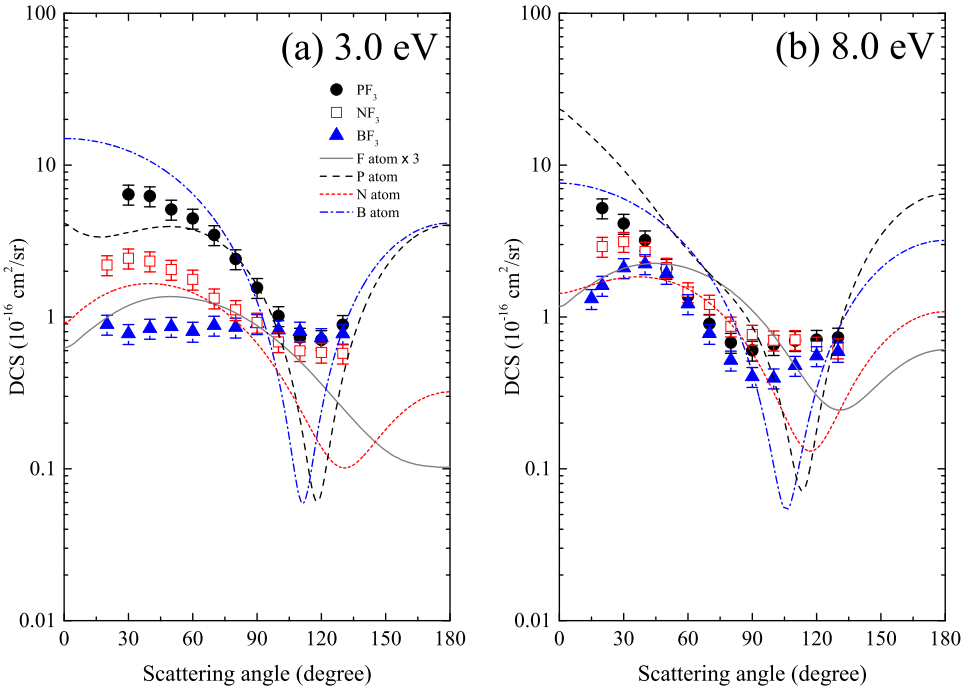


FIG. 4. Contributions of elastic DCSs from the central X (X = B, N, and P) atoms and fluorine atoms multiplied by factor of three (F × 3) in those for $XF_3$ molecules at impact energies of (a) 3.0 eV and (b) 8.0 eV (see legends for details).

the scattering angles from 80° to 130° become shallower for $PF_3$ and $NF_3$. However, for large angles above 100°, the calculated cross sections at this energy tend to increase in magnitude and deviate from the observed angular distribution. Note that above 130°, there is no experimental evidence to compare with the backward scattering DCS values predicted by the theory. As shown in Fig. 4(b), the experimental DCSs of the studied molecules start reflecting an atomic-like behavior as that calculated with the IAM-SCAR approach for incident energies around 8.0 eV.

Finally, as expected, measured DCS values for the three considered molecules converge on a single shape, within the experimental uncertainty limits, when the energy increases up to 100 eV, showing an excellent agreement with the corresponding IAM-SCAR calculation for $XF_3$ molecules and atomic F (×3) [see Fig. 3(d)]. We found a similar behavior for non-polar molecules such as $CF_4$, $SiF_4$, and $GeF_4$ (see Ref. 12), thus providing strong evidence of the important contribution of the constituent atoms to the electron scattering from these molecular symmetries (atomic like behaviour). This also indicates the convenience of using in these cases relatively simple approaches versus full scattering treatments such as the R-matrix code.[2] The IAM-SCAR method is providing here a reasonable description of the electron scattering from these molecular species. In particular, as derived from the above comparison, for heavy constituent atoms, like the P atom in $PF_3$, the validity of the screening corrected additivity rule could be extended down to 2.0 eV.

### C. Total, integral, and momentum-transfer cross sections for $e^-$ + $PF_3$

The elastic ICS and MTCS as well as the inelastic ICS and electron scattering TCS obtained from the present analysis are shown in Figs. 5(a) and 5(b), respectively, together with other previous experimental and theoretical results available in the literature.[2,6,8] The present DCSs shown in Fig. 2 were extrapolated according to the procedure described in Sec. III and then integrated, in order to derive the corresponding ICS values which are shown at the bottom in Table II and plotted in Fig. 5(a). Our IAM-SCAR-calculated elastic ICS,

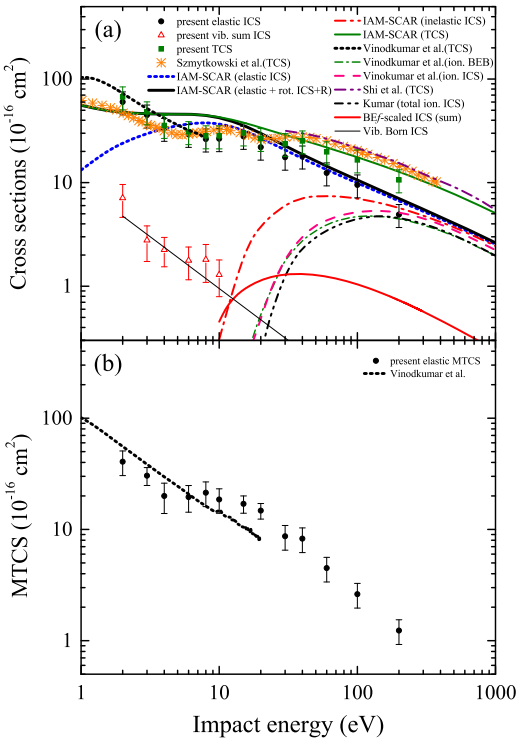


FIG. 5. (a) The total, elastic, and inelastic integral cross sections for $PF_3$ together with previous data in the literatures. (b) The elastic momentum-transfer cross sections (see legends for details).

inelastic (electronic excitation plus ionization) ICS, and electron scattering TCS are also plotted in this figure for comparison. Note that the calculated TCS does not include the vibrational excitation cross section which is plotted separately [see Fig. 5(a)].

Furthermore, *experimental* TCS values have been estimated by adding the IAM-SCAR total inelastic ICS (including the rotational, electronic excitations, and ionization) to the sum of our experimental $v_1$, $v_2$, $v_3$, and $v_4$ composed vibrational excitation ICSs (see Ref. 14) and our elastic ICS. The corresponding results are also shown in Fig. 5(a).

As shown in this figure and as expected from our previous discussion at the DCS-level, our experimental and theoretical elastic ICS are in quite good agreement with one another, to within the experimental uncertainties, for impact energies between 20 and 200 eV. Below 10 eV, however, the current IAM-SCAR calculation does not reproduce the experimental energy dependence of the elastic ICS. At these low energies, our measured ICSs track well the trends of the TCS data measured by Szmytkowski *et al.*[6] and the R-matrix calculation by Vinodkumar *et al.*[2] Although the TCS calculated by the R-matrix code[2] is about 11% systematically higher than our experimental data, this is probably because of the different methods used to account for the rotational excitation cross sections (see the above discussion on the DCS values), although this difference is less than the combined uncertainty limits. In principle, any ICS value should not exceed the magnitude of the corresponding TCS. However, our experimental vibrationally elastic ICS (black circles in Fig. 5) was found to be slightly larger in magnitude than the experimental TCS of Szmytkowski *et al.*[6] As mentioned above, our dipole-Born extrapolation of the DCS for small angles included dipole rotational excitations ($J = 0 \rightarrow 1$) which are not distinguishable within the experimental conditions of Ref. 6 which explains why our "experimental TCS" can be higher than the experimental TCS data.[6] We note here that our elastic ICS using only the MPSA-fitting *without the dipole-Born extrapolation* already overestimates at 2.0 and 3.0 eV. Though the discrepancy is still within a tolerance of ~28%, further confirmation would be still desirable with better angular and energy resolution TCS measurements paying special attention to the forward scattering correction due to the polar molecules with a large dipole moment. Our "experimental TCS" (derived from the addition procedure described above) for energies below 10 eV gives a similar value to our elastic ICS, probably because of the small contribution from the vibrational ICS for the composed fundamental modes. The two resonances at 0.78 eV and 13.6 eV theoretically predicted in Ref. 2 can be identified with the present increasing cross section values for the lower energies and the local maximum around 10 eV, respectively. The first resonance is ascribed to the E representation, and the second to the $A_1$ representation leading to negative ion formation ($PF_2^-$ at 10.3 eV, $F_2^-$ at 10.9 eV, and $PF^-$ at 11.4 eV[4]).

Other integral cross section values available in the literature have also been plotted in order to provide a more complete database for modeling purposes: Integral vibrational excitation cross sections from the sum of the present $v_1$, $v_2$, $v_3$, and $v_4$-vibrational fundamental modes, electronic excitation from the sum of the Binary-Encounter-*f* (BE*f*)-scaled Born ICSs for tow low-lying optically allowed transitions of $8a_1^{-1} \rightarrow 7e$ ($\sigma^*$) and $8a_1^{-1} \rightarrow 4s$ discrete excitations as well as three different ionization ICS data derived from the CSP-IC and the binary encounter Bethe methods by Vinodkumar *et al.*,[2] and from the modified Jain-Khare semi-empirical approach by Kumar.[9] There is a general agreement between the three ionization cross section datasets, and the consistency between the inelastic cross section data plotted in Fig. 5(a) is proved by the good agreement between the IAM-SCAR inelastic cross section and the sum of the averaged ionization cross sections with the present BE*f*-scaled electronic excitation ICS.

Finally, the elastic MTCS is shown in Fig. 5(b), together with the recent R-matrix calculation from Ref. 2. These MTCS data are very useful for modeling electron transport in order to estimate electron properties when they drift and diffuse, under the influence of an applied electric field or crossed electric and magnetic fields, through gases.

## V. CONCLUSION

We reported for the first time a compilation of experimental elastic differential, integral, and momentum-transfer cross sections for electron scattering from $PF_3$ molecules in the impact energy range from 2.0 to 200 eV. Corresponding theoretical elastic as well as inelastic (electronic excitation plus ionization) cross sections obtained with the IAM-SCAR method were also presented together with additional rotational excitation cross section calculated within the framework of the Born approximation. As expected from previous studies, fairly good agreement has been found between our experimental and theoretical elastic DCS and ICS data for energies higher than about 20 eV. Below 10 eV, our elastic IAM-SCAR calculation, including rotational excitations, also showed an acceptable agreement, within the uncertainty limits, both at the DCS and ICS levels. A calculation using the R-matrix code[2] also provides reliable cross sections for this low energy range except for the rotational excitation ($J = 0 \rightarrow 1$) which was clearly overestimated as deduced from the large value of the calculated dipole moment with respect to the experimental one. In addition, comparisons of elastic DCSs for other three-fluorine containing $BF_3$ and $NF_3$ molecules, along with our corresponding IAM-SCAR results, have been made to illustrate molecular systematics in their elastic scattering characteristics. The present inelastic scattering ICSs, discrete electronic-state excitation plus ionization, were found to be consistent with three independent sets of ionization ICS calculations found in the literature. Present "experimental TCS" values obtained by adding our inelastic IAM-SCAR calculation with the sum of the observed vibrational excitation cross sections and our measured vibrational plus elastic ICS were also found to be largely consistent with the available TCS measurements. Finally, we provided, at the current level, a useful evaluated cross section dataset including all the present measurements and those available in the literature. Details on inelastic processes, especially vibrational and electronic excitations, for the $e^- + PF_3$ collisional system will be discussed in a sequel paper (Part II).[14]

## ACKNOWLEDGMENTS

This work was conducted under the support of the Ministry of Education, Culture, Sports, Science and Technology-Japan. F.B. and G.G. acknowledge the partial financial support from the Spanish Ministerio de Economia y Competitivided (Project No. FIS 2012-31230).

[1] M. Hoshino, P. Limão-Vieira, A. Suga, H. Kato, F. Ferreira da Silva, F. Blanco, G. García, and H. Tanaka, J. Chem. Phys. **143**, 024313 (2015).
[2] M. Vinodkumar, C. Limbachiya, H. Desai, and P. C. Vinodkumar, Phys. Rev. A **89**, 062715 (2014).
[3] K. A. G. MacNeil and J. C. J. Thynne, J. Phys. Chem. **74**, 2257 (1970).
[4] P. W. Harland, D. W. H. Rankin, and J. C. J. Thynne, Int. J. Mass Spectrom. Ion Phys. **13**, 395 (1974).
[5] D. F. Torgerson and J. B. Westmore, Can. J. Chem. **53**, 933 (1975).
[6] C. Szmytkowski, M. Piotrowicz, A. Domaracka, L. Klosowski, E. Ptasinska-Denga, and G. Kasperski, J. Chem. Phys. **121**, 1790 (2004).
[7] J. W. Au, G. Cooper, and C. E. Brion, Chem. Phys. **215**, 397 (1997).
[8] D. H. Shi, J. F. Sun, Z. L. Zhu, and Y. F. Liu, Eur. Phys. J. D **57**, 179 (2010).
[9] R. Kumar, J. Appl. Math. Phys. **3**, 1671 (2015).
[10] M. Hoshino, P. Limão-Vieira, K. Anzai, H. Kato, H. Cho, D. Mogi, T. Tanioka, F. Ferreira da Silva, D. Almeida, F. Blanco, G. García, O. Ingólfsson, and H. Tanaka, J. Chem. Phys. **141**, 124302 (2014).
[11] H. Murai, Y. Ishijima, T. Mitsumura, Y. Sakamoto, H. Kato, M. Hoshino, F. Blanco, G. García, P. Limão-Vieira, M. J. Brunger, S. J. Buckman, and H. Tanaka, J. Chem. Phys. **138**, 054302 (2013).
[12] H. Kato, A. Suga, M. Hoshino, F. Blanco, G. García, P. Limão-Vieira, M. J. Brunger, and H. Tanaka, J. Chem. Phys. **136**, 134313 (2012).
[13] P. Limão-Vieira, M. Horie, H. Kato, M. Hoshino, F. Blanco, G. García, S. J. Buckman, and H. Tanaka, J. Chem. Phys. **135**, 234309 (2011).
[14] N. Hishiyama, M. Hoshino, F. Blanco, G. García, and H. Tanaka, "Absolute cross section measurements for the scattering of low- and intermediate-energy electrons from $PF_3$. II. Inelastic scattering of vibrational and electronic excitations," J. Chem. Phys. (unpublished).
[15] H. Tanaka, L. Boesten, D. Matsunaga, and T. Kudo, J. Phys. B: At., Mol. Opt. Phys. **21**, 1255 (1988).
[16] H. Kato, T. Asahina, H. Masui, M. Hoshino, H. Tanaka, H. Cho, O. Ingólfsson, F. Blanco, G. Garcia, S. J. Buckman, and M. J. Brunger, J. Chem. Phys. **132**, 074309 (2010).
[17] H. Tanaka, T. Ishikawa, T. Masai, T. Sagara, L. Boesten, M. Takekawa, Y. Itikawa, and M. Kimura, Phys. Rev. A **57**, 1798 (1998).
[18] T. Shimanouchi, *Tables of Molecular Vibrational Frequencies, Consolidated Volume I*, National Standard Reference Data Series 39 (National Bureau of Standards, 1972), p. 17.
[19] J. N. H. Brunt, G. C. King, and F. H. Read, J. Phys. B: At., Mol. Opt. Phys. **10**, 1289 (1977).
[20] S. F. Wong and A. L. Dube, Phys. Rev. A **17**, 570 (1978).
[21] L. Boesten and H. Tanaka, At. Data Nucl. Data Tables **52**, 25 (1992).
[22] S. K. Srivastava, A. Chutjian, and S. Trajmar, J. Chem. Phys. **63**, 2659 (1975).
[23] R. T. Brinkmann and S. Trajmar, Rev. Sci. Instrum. **14**, 245 (1981).
[24] J. C. Nickel, P. W. Zetner, G. Shen, and S. Trajmar, J. Phys. E: Sci. Instrum. **22**, 730 (1989).
[25] F. Rugamas, D. Roundy, G. Mikaelian, G. Vitug, M. Rudner, J. Shih, D. Smith, J. Segura, and M. A. Khakoo, Meas. Sci. Technol. **11**, 1750 (2000).
[26] F. Blanco and G. García, Phys. Lett. A **360**, 707 (2007).
[27] F. Blanco, J. Rosado, A. Illana, and G. García, Phys. Lett. A **374**, 4420 (2010).
[28] L. Boesten and H. Tanaka, J. Phys. B: At., Mol. Opt. Phys. **24**, 821 (1991).
[29] D. G. Thompson, J. Phys. B: At., Mol. Opt. Phys. **4**, 468 (1971).
[30] G. G. Raju, IEEE Trans. Dielectr. Electr. Insul. **16**, 1199 (2009).
[31] Y. Itikawa, Phys. Rev. A **3**, 831 (1971).
[32] B. H. Bransden and C. J. Joachain, *Physics of Atoms and Molecules* (Longmans, London, 1983).
[33] T. Shimanouchi, J. Phys. Chem. Ref. Data **6**, 993 (1977).
[34] *CRC Handbook of Chemistry and Physics*, 92nd ed., edited by W. M. Haynes (CRC Press, Boca Raton, London, New York, 2011-2012).
[35] See http://webbook.nist.gov/chemistry/ for the physical properties of the molecules.
[36] L. Boesten, Y. Tachibana, Y. Nakano, T. Shinohara, H. Tanaka, and M. A. Dillon, J. Phys. B: At., Mol. Opt. Phys. **29**, 5475 (1996).
[37] M. Matsui, M. Hoshino, H. Kato, F. Ferreira da Silva, P. Limão-Vieira, and H. Tanaka, Eur. Phys. J. D **70**, 77 (2016).
[38] W. L. Jolly, *Modern Inorganic Chemistry* (McGraw-Hill, 1984), pp. 77–90.
[39] D. F. Pastega, R. F. da Costa, M. A. P. Lima, and M. H. F. Bettega, Eur. Phys. J. D **68**, 20 (2014).